Stochastic Environmental Research and Risk Assessment
https://doi.org/10.1007/s00477-025-03114-w

ORIGINAL PAPER

Study on the joint distribution of air temperature, solar radiation, and wind speed in the complex mountainous bridge sites based on field measurement

Mingjin Zhang[1,2] · **Jiale Long**[1,2] · **Jingxi Qin**[3] · **Jinxiang Zhang**[1,2] · **Xulei Jiang**[2,4] · **Yongle Li**[1,2]

Received: 1 March 2025 / Accepted: 11 September 2025

Abstract
In complex mountainous areas with high mountains and deep valleys, bridge sites are prone to strong winds, solar exposure, abrupt air temperature changes, and other extreme natural conditions, leading to more severe and complex environmental loads on bridge structures compared to plain areas. Current design specifications do not consider solar radiation when calculating uniform temperature, and the simple superposition of extreme air temperature and wind effects leads to an overestimation of combined loads since their extreme values rarely occur simultaneously. Therefore, a comprehensive study on the joint distribution of air temperature, solar radiation, and wind in complex mountainous areas is necessary. This study uses environmental parameter data from field measurements in complex mountainous bridge sites to establish joint distribution models of air temperature, solar radiation, and wind speed based on the Copula functions. The joint distribution models are used to calculate the joint values of air temperature, solar radiation, and wind speed actions under the different return periods, which are subsequently converted to extreme temperature action values for bridge structures. A reduction coefficient of temperature action is proposed to reflect the differences in temperature action values between univariate and multivariable return periods. This research offers a practical reference for determining temperature design loads for long-span bridges in complex mountainous areas.

Keywords Field measurements · Copula functions · Return periods · Joint values · Temperature action values · Reduction coefficient

1 Introduction

The bridge sites in complex mountainous areas are often prone to severe storms, prolonged solar exposure, abrupt air temperature changes, and other extreme natural conditions. The environmental loads of the bridge structures in these areas are more intense and complex than those in plain areas. When designing long-span bridges in these areas, it is essential to comprehensively consider the impact of extreme environmental parameters, particularly air temperature, solar radiation, and wind, which are often correlated (Valipour 2015; Abid et al. 2022). Changes in ambient air temperature, solar radiation, and wind can significantly affect the temperature field in structures (Emerson 1976). Therefore, field measurement and analysis of these parameters are crucial for determining design load values of long-span bridges in complex mountainous areas.

In studies related to the field-measured wind environmental parameters at bridge sites, scholars have mainly focused on wind parameters such as wind speed, attack angle, gust factor, turbulence intensity, and turbulence integral scale with the ultimate goal of evaluating their effects on bridge structural loads and dynamic responses (Li et al.

✉ Jingxi Qin
jingxi.qin@polyu.edu.hk

1 State Key Laboratory of Bridge Intelligent and Green Construction, Southwest Jiaotong University, Chengdu 611756, China

2 Department of Bridge Engineering, Southwest Jiaotong University, Chengdu 610031, China

3 Department of Civil and Environmental Engineering, The Hong Kong Polytechnic University, Hong Kong, China

4 Zhejiang Institute of Communications Co., Ltd, Hangzhou 310030, China

Published online: 17 October 2025

2015; Yu et al. 2019; Liao et al. 2020; Zhang et al. 2021b; Fenerci et al. 2017). However, none of these factors considers the load effects of air temperature and solar radiation on the structure, and the actual combined loads on the structure are difficult to determine. Solar radiation and air temperature are generally interrelated. In studies related to the actions of air temperature and solar radiation on bridge structures based on field measurements, Chen et al. (2012) studied the impact of solar radiation and environmental air temperatures on environmental thermal effects and established a two-dimensional heat transfer model for the temperature variation of the bridge tower over time. Abid et al. (2016) constructed a large concrete box girder segment and installed sensors to measure temperature and solar radiation. They also proposed an empirical formula to predict the maximum vertical temperature gradient at the top surface of concrete superstructures. Dilger et al. (1983) predicted the temperature distribution in composite beam bridges by analyzing the diurnal temperature difference of structures exposed to solar radiation and summarized the temperature stress distribution in box sections under the most unfavorable temperature field. However, wind has a significant impact on the study of the aforementioned thermal effects and has not been considered.

The abovementioned literature mainly focuses on wind characteristics or thermal effect characteristics of air temperature and solar radiation individually, and the discussion on the joint effects of measured air temperature, solar radiation, and wind speed is absent, with even fewer measurements taken in mountainous areas. To explore the effect of the combined air temperature, solar radiation, and wind speed on temperature action values of bridges in complex mountainous areas, establishing the joint distribution of air temperature, solar radiation, and wind models based on field-measured data is necessary. An effective strategy for establishing multi-parameter joint distribution models is based on the Copula theory, first introduced by Sklar (1959) to describe the correlation between multiple variables and provide an appropriate tool for calculating multivariate joint distributions. It splits the joint distribution of multiple variables into the marginal distributions of independent variables and the Copula function that connects them based on the decomposition idea. The Copula theory has been further refined in recent decades (Kampé de Fériet 1973; Genest and Rivest 1993; Nelsen 2006) and applied in numerous research fields. In wind engineering research, many scholars have used various Copula functions to study the correlations between wind speed, wind direction, angle of attack, and turbulence intensity (Chen et al. 2022; Zhang et al. 2022, 2023a, b; Huang et al. 2023). In the field of temperature research, some researchers have also used copula functions to establish joint probability models for solar radiation, environmental temperature, sunshine duration, and temperature difference (Yet et al. 2019; Panamtash et al. 2020; Abraj and Hewaarachchi 2021; Zhang et al. 2021a; Ramírez et al. 2021). Currently, there are few studies utilizing Copula theory for joint analysis of air temperature, solar radiation, and wind speed. Moreover, the applicability of this approach to multiple environmental parameters in mountainous regions remains to be thoroughly evaluated.

Moreover, these environmental parameters rarely reach extreme values simultaneously, making it essential to consider their combined effects. Current specifications (European Committee for Standardization 2004; Ministry of Transport of the People's Republic of China 2015; American Association of State Highway and Transportation Officials 2020) overlook the impact of solar radiation on temperature distribution in mountainous regions and neglect its contribution to uniform temperature calculations. Furthermore, the simple superposition of air temperature and wind loads often results in overestimated combined loads, leading to conservative structural design and high construction costs. The varying regularity of temperature actions on bridges in mountainous sites under the combined influence of air temperature, solar radiation, and wind speed still needs further clarification. Therefore, it is necessary to establish a joint distribution model considering multiple environmental parameters to provide a reference for the design loads of long-span Bridges in mountainous areas.

The remaining sections of this paper are as follows. Section 2 introduces the methodology, including concepts such as marginal distribution models, Copula functions, the most-likely combination value, and return periods. Section 3 describes the data sources and provides preliminary analysis and classification. Section 4 presents the results and discussion of the data analysis, and Sect. 5 summarizes the main conclusions of this study.

2 Methodology of the joint distribution of air temperature, solar radiation, and wind speed

This section primarily introduces the methodology for investigating the joint distribution of temperature, solar radiation, and wind speed. Figure 1 shows a step-by-step schematic for the study.

This study utilizes environmental parameter data from field measurements in complex mountainous bridge sites for data segmentation and statistical analysis. We then establish joint distribution models of extreme air temperature and its corresponding solar radiation and wind speed using various Archimedean Copula functions. These models are used to derive the joint values of air temperature and

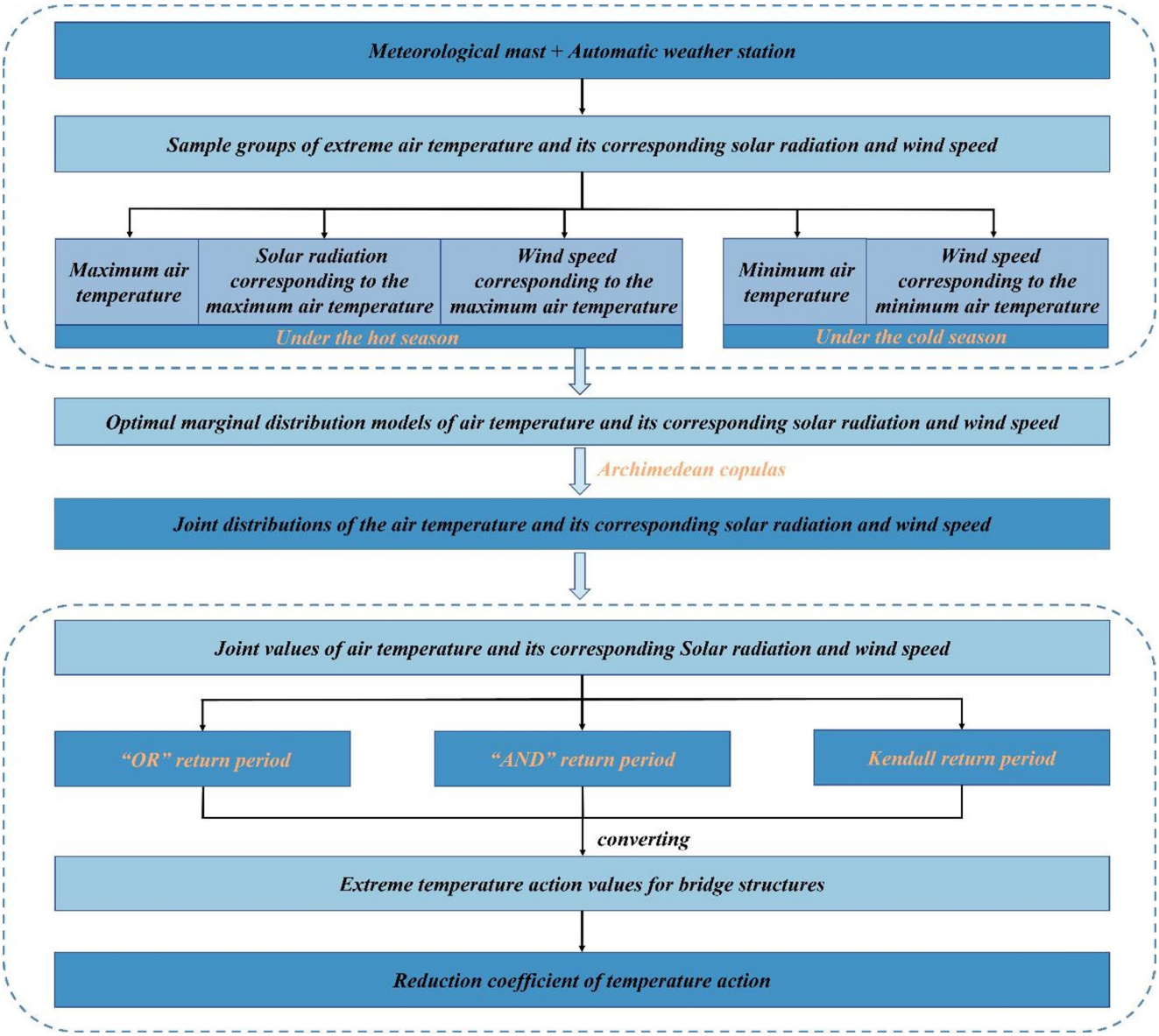

Fig. 1 Flowchart of the joint distribution study of air temperature, solar radiation, and wind speed

its corresponding solar radiation and wind speed under different return periods, which are subsequently converted to extreme temperature action values for bridge structures. Finally, a reduction coefficient of temperature action is proposed to reflect the differences in temperature action values between univariate and multivariate return periods.

2.1 The marginal distribution models of air temperature, solar radiation, and wind speed

The premise of establishing a reliable joint distribution model of environmental parameters is to determine the most suitable marginal distribution models for each environmental parameter. The distribution model for extreme environmental parameters varies across areas and types, with no definitive conclusion on its applicability (Riera and Nanni 1989). The commonly used distribution model and its probability density function (PDF) and cumulative distribution function (CDF) are listed in Table A1 in the Appendix, including the Generalized Extreme Value distribution (Jenkinson 1955), Log-Normal distribution, Gamma distribution, and Logistic distribution. This research will first test the applicability of these distribution models to the samples of the measured air temperature, solar radiation, and wind speed in the study area. The parameters of the distribution model were determined using the maximum likelihood estimation (MLE) method (Casella and Berger 2024).

2.2 The joint distribution of air temperature, solar radiation, and wind speed

After obtaining the optimal marginal distribution models for air temperature, solar radiation, and wind speed during hot and cold seasons, the Archimedean Copula family was used to construct the joint distributions of air temperature, solar radiation, and wind speed.

2.2.1 Archimedean copula family

The Archimedean Copula family is a type of Copula function used to model and analyze the dependence relationships among multivariate random variables (Genest and Mackay 1986). It simplifies complex dependence issues into univariate problems and converges quickly, making it widely applicable. This study employs the Clayton, Frank, and Gumbel Copulas (Nikoloulopoulos 2013) to establish the joint distribution of environmental parameters. These three Copula functions can completely describe the characteristics of environmental data (Li et al. 2016; Yin et al. 2017), including upper tail dependence, lower tail dependence, and symmetric dependence. A detailed description of these three copulas can be found in Table A2 in the Appendix.

2.2.2 Parameter estimations of copula functions

The key step of establishing the Copula model is the determination of parameters, and the correct parameters play a decisive role in the Copula model. This study utilizes the relationship between the Kendall rank correlation coefficient and the generator function φ of the Copula function to deduce the parameter$\theta$of the Copula function. The Kendall rank correlation coefficient measures the strength of monotonicity between two variables, determined.

as follows:

$$\tau = \frac{P-Q}{N(N-1)/2} = \frac{4P}{N(N-1)} - 1 \tag{1}$$

where P denotes the number of concordant pairs(two samples (x_i,y_i), (x_j,y_j), when $x_i > y_i$, then $x_j > y_j$ or when $x_i < y_i$, then $x_j < y_j$), Q denotes the number of discordant pairs(two samples (x_i,y_i), (x_j,y_j), when $x_i > y_i$, then $x_j < y_j$ or when $x_i < y_i$, then $x_j > y_j$), and N represents the number of statistical objects.

The relationship between the Kendall rank correlation coefficient τ and the generator function$\varphi$of the Copula is defined as follows:

$$\tau = 1 + 4\int_0^1 \frac{\varphi(t)}{\varphi'(t)}dt \tag{2}$$

where $\varphi'(t)$ is the first derivative of $\varphi(t)$.

Through Eq. (2), the relationships between the Kendall rank correlation coefficient τ and the three typical Archimedean Copula parameters$\theta$are shown in Table 1.

The parameters of the bivariate Copula functions are estimated using Eq. (1) to Eq. (5), while the parameters of the trivariate Copula functions are estimated using the MLE method described in Sect. 2.1.

2.3 Goodness-of-fit evaluation metrics

For the marginal distribution models of air temperature, solar radiation, and wind speed, the Kolmogorov–Smirnov test (K–S test), the coefficient of determination (R^2), the root mean square error (RMSE), and the Bayesian information criterion (BIC) are commonly used to assess the goodness-of-fit of the target parameters.

The Kolmogorov–Smirnov (K–S) test evaluates the consistency between the empirical distribution $F_n(x)$ and the theoretical distribution $F_0(x)$ by measuring their maximum divergence D, defined as:

$$D = \sup_x |F_n(x) - F_0(x)| \tag{6}$$

where the operator sup (supremum) denotes the least upper bound of absolute differences across all observed data points. The null hypothesis H_0 states that the sample data distribution conforms to the assumed distribution function. The hypothesis is accepted if the distance value $D < D(n,\alpha)$ or the p-value $p > \alpha$(α is the significance level (typically set at 0.05) and p is the probability of the null hypothesis being true).

For the Copula joint distribution models of air temperature, solar radiation, and wind speed, the evaluation metrics listed in Table A3 are used to assess the fitting performance.

Table 1 The relationship between the Kendall rank correlation coefficient and the parameters of copula functions

Copula functions	The relationship betweenτandθ	
Clayton	$\tau = \frac{\theta}{2+\theta}$	(3)
Frank	$\tau = 1 + \frac{4}{\theta}[\frac{1}{\theta}\int_0^\theta \frac{t}{\exp(t)-1}dt - 1]$	(4)
Gumbel	$\tau = 1 - \frac{1}{\theta}$	(5)

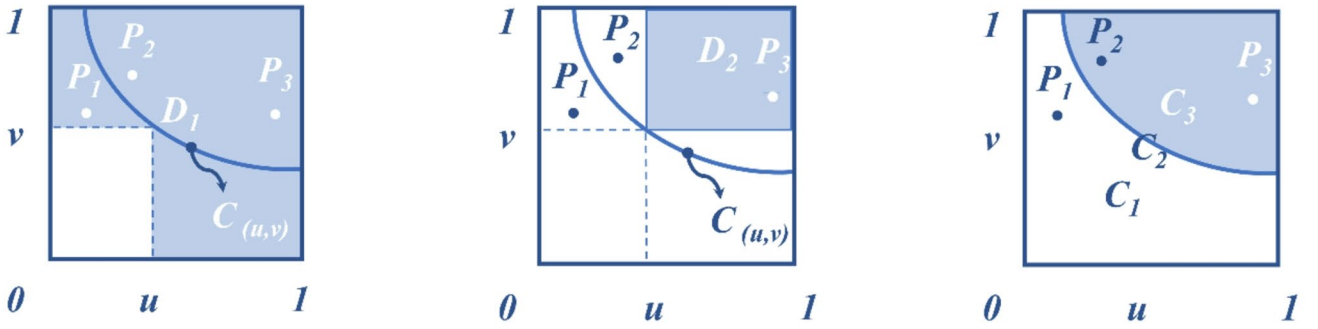

(a) "OR" return period (b) "AND" return period (c) The Kendall return period

Fig. 2 Multivariate return periods

2.4 The joint values of air temperature, solar radiation, and wind speed under return periods

This section introduces the concepts of univariate and multivariate return periods for the comparative analysis of temperature effect values in the following sections.

2.4.1 Univariate return period

The univariate return period is the average interval between two consecutive occurrences of a specified event. Assuming that a random variable follows a distribution $F_X(\mathrm{x})$, then the expression of the univariate return period $T(x)$ is:

$$T(x) = \frac{\lambda_T}{1 - P(X \leqslant x)} = \frac{\lambda_T}{1 - F_X(x)} \tag{7}$$

where$\lambda_T$is the time interval between events.

2.4.2 Multivariate return periods

Under the bivariate joint distribution$C(u, v)$, the return period corresponding to either variable exceeding a specific value is called the "OR" return period, and the return period associated with both variables simultaneously exceeding a specific value is called the "AND" return period. The Kendall return period. To solve the limitations of the above two traditional return periods, Salvadori et al. (2013) proposed the concept of the Kendall return period, which defines hazardous regions of return periods based on joint distribution values. The expressions for the above multivariate return periods are provided in Table A4 of the Appendix.

As illustrated in Fig. 2, the blue area represents the hazardous zone. For events P_1 and P_2, both the "OR" return period and the "AND" return period may lead to misjudgments in engineering event assessment. In contrast, the Kendall return period provides a more reasonable and reliable estimate for event evaluation.

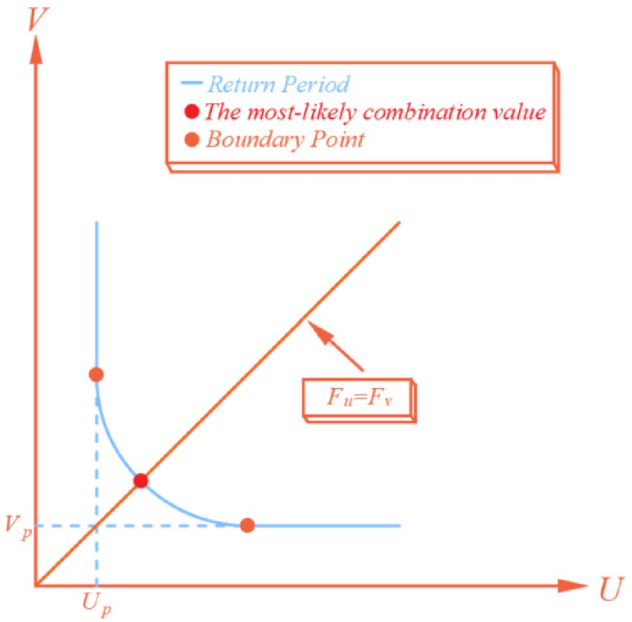

Fig. 3 The definition of the most-likely combination value

2.4.3 The most-likely combination values of air temperature, solar radiation, and wind speed

Salvadori et al. (2015) introduced the concept of "most-likely combination value" for multivariate return periods, which identifies the most probable situation on a contour line or surface, as shown in Fig. 3. The most-likely combination value occurs at the intersection of the line where the distribution functions of the random variables U and V are equal (F_u=F_v) and the contour line of the return period, where the joint probability density function *f (u, v)* attains its maximum. This approach is applied to determine the joint values of air temperature, solar radiation, and wind speed for different return periods during hot and cold seasons.

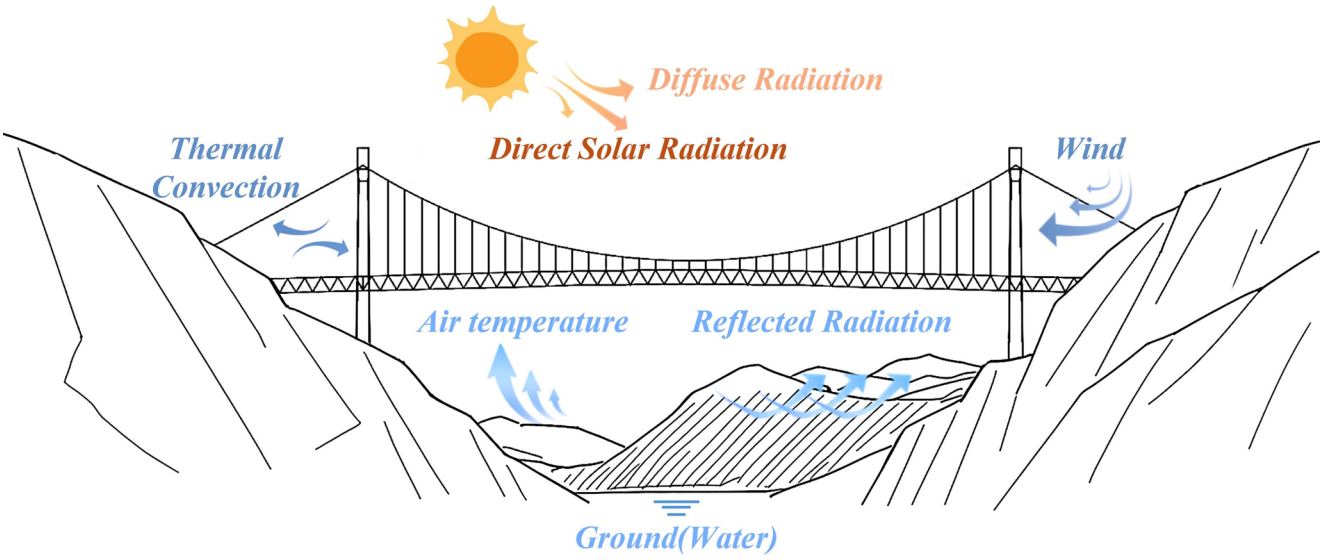

Fig. 4 The thermal environment in which the bridge structure is located

Table 2 The temperature actions on Bridge structures

	Maximum temperature action value		Minimum temperature action value	
Steel bridges with steel deck slabs	$T_{g,e1} = 38.00 + \frac{T_t - 20}{2.00}$	(8)	$T_{d,e1} = -1.48 + \frac{T_t}{0.91}$	(9)
Steel bridges with concrete deck slabs	$T_{g,e2} = 28.23 + \frac{T_t - 20}{1.44}$	(10)	$T_{d,e2} = -0.12 + \frac{T_t}{1.21}$	(11)
Concrete bridges and stone bridges	$T_{g,e3} = 24.14 + \frac{T_t - 20}{1.40}$	(12)	$T_{d,e3} = \frac{T_t + 1.85}{1.58}$	(13)

2.5 Temperature actions of bridge structures

As illustrated in Fig. 4, environmental loads on bridge structures in mountainous areas involve multiple factors. The temperature action value is defined as the structure's comprehensive response to environmental thermal effects. This study converts the joint values of air temperature, solar radiation, and wind speed under various return periods into extreme temperature action values based on the Chinese specification(Ministry of Transport of the People's Republic of China 2015). The impact of multiple environmental parameters on bridge temperature effects is then examined using a proposed temperature action reduction coefficient.

2.5.1 Temperature action value

According to the Chinese specification, the maximum and minimum temperature actions on bridge structures with different materials can be determined based on the local ambient temperature, as shown in Table 2.

where T_t represents the air temperature. For concrete structures, it is the local historical highest daily average temperature or lowest daily average temperature, and for steel structures, it is the local historical highest temperature or lowest temperature. The negative value will be taken when the temperature is below 0 °C.

2.5.2 The reduction coefficient of temperature action

To investigate the variation of the temperature action values on the bridge structure under multivariate return periods, the temperature action reduction coefficient is defined asα, and its expression is as follows:

$$\alpha = \frac{\Delta T_1}{\Delta T_0} = \frac{T_D - T_{mean}}{T_M - T_{mean}} \tag{14}$$

where ΔT_1 represents the difference between the extreme value and the mean value of temperature action on the bridge structure under the multivariate return period,ΔT_0 represents the difference between the extreme value and the mean value of temperature action on the bridge structure under the univariate return period. T_D and T_M represent the temperature action values for bridge structures under multivariate and univariate return periods, respectively. T_{mean} represents the mean value of temperature action on the bridge structure under the univariate return period.

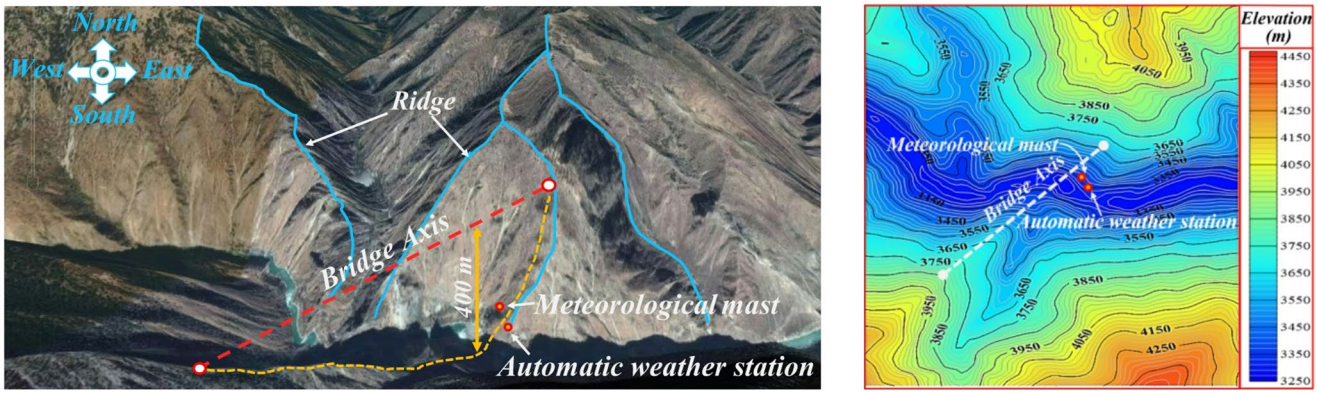

(a) Topographic map (b) Contour map

Fig. 5 The topography and geomorphology surrounding the research area

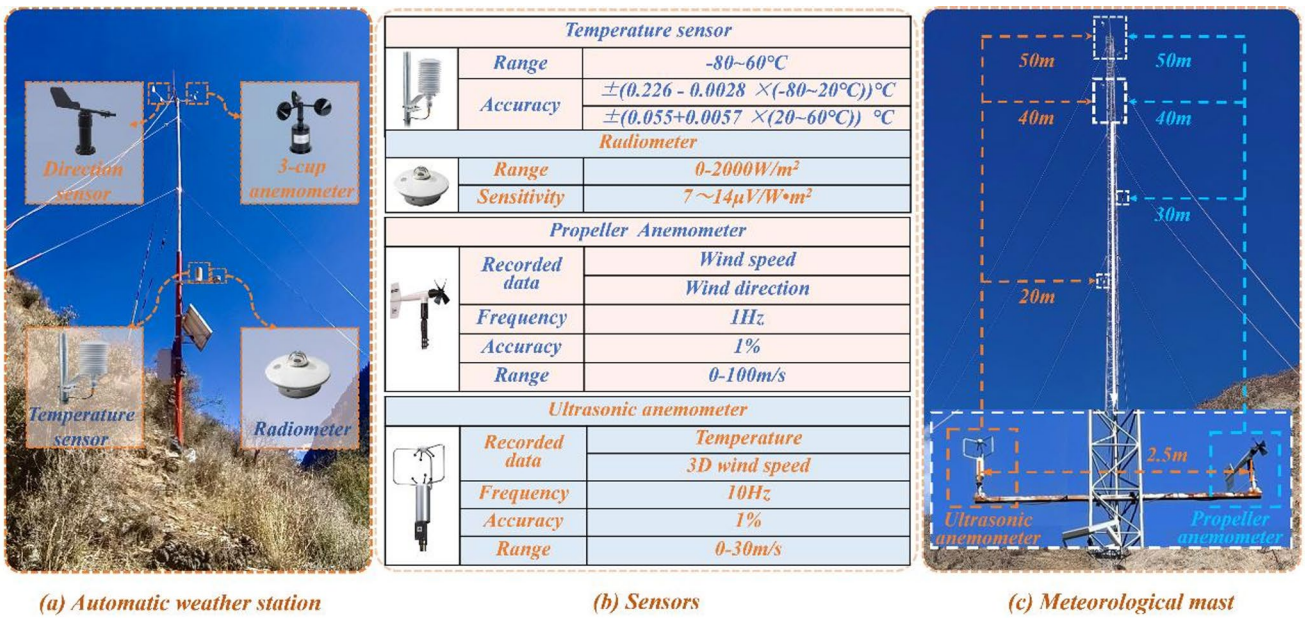

(a) Automatic weather station (b) Sensors (c) Meteorological mast

Fig. 6 Layout of the field measuring devices

3 Data sources

In complex mountainous areas with undulating terrain and variable climate, the distribution of air temperature, solar radiation, and wind speed is strongly affected by topography, altitude, and local circulation. These unique climatic features directly influence the temperature field of bridge structures. Hence, installing environmental monitoring devices is essential to support large-span bridge construction in such regions.

3.1 Research area and measuring system

The research area was located in a typical high-altitude V-shaped deep canyon, as shown in Fig. 5. The bridge spans from the southwest to the northeast, with the deck situated at an altitude of approximately 3800 m and about 400 m above the canyon floor. The bridge site area features criss-crossing valleys and significant terrain undulations, coupled with complex and variable weather conditions and frequent extreme weather events, which greatly impact the bridge. Therefore, the monitoring system is deployed near the transverse side of the bridge, at a vertical height of about 300 m, to collect environmental parameters.

A 10 m high CAWS600-RT six-element automatic weather station (AWS) and a 50 m high meteorological mast have been installed in the research area to collect environmental parameter data. Figure 6 provides a detailed description of the sensors installed on the automatic weather station and the meteorological mast. The design for the anemometers and the meteorological mast follows the provisions specified in the International Electrotechnical Commission

(IEC) 61400-50-1:2022 (International Electrotechnical Commission (IEC) 2022). According to the provision, regarding the optimal mounting orientation, the lateral layout of the anemometers should be oriented perpendicular to the prevailing wind in the canyon to minimize wake effects from both the meteorological mast and nearby anemometers, ensuring reliable wind speed measurements. Further, the guideline emphasizes that meteorological masts should maximize flow permeability to reduce wake effects on anemometers and ensure measurement accuracy and reliability. Moreover, the mast flow distortion should be under 1%. In our setup, the triangular lattice mast is installed perpendicularly to the predominant wind direction, and has a high permeability of 0.82. The ultrasonic and propeller anemometers were mounted at the same height, separated by 2.5 m (each positioned 1.25 m from the mast center). The mast leg spacing is 0.5 m, and the mast-to-sensor distance exceeds 2.5 times the leg spacing. Given the setup of the mast, the flow distortion rate is below 1%. The design fully satisfies the recommended requirement and provides a practical balance between minimizing wake effects and maintaining structural stability, ensuring reliable wind measurements.

To confirm the reliability of this spacing setup, cross-validation measurements were conducted at the same site, where the two anemometers were directly compared. As shown in Fig. 7, the daily wind speed records from the ultrasonic and propeller anemometers were highly consistent, with no abnormal discrepancies observed, thereby verifying that the 2.5 m separation between the instruments provides dependable wind speed measurements.

3.2 Data processing and classification

The measurement period spans two years, during which a comprehensive dataset of environmental parameters was collected. This study primarily utilized air temperature data collected by the temperature sensor mounted on the automatic weather station near the meteorological mast where ultrasonic anemometers are installed. The air temperature data recorded by the ultrasonic anemometer at the 20 m height is generally more continuous and complete, although it is subject to inaccuracies due to virtual temperature effects. To address this limitation, the ultrasonic anemometer data is used to fill in the missing values of the temperature sensor in the automatic weather station, providing a more comprehensive and reliable temperature dataset. Due to the proximity of the AWS to the meteorological mast, the temperature measurements from both sites exhibit strong spatial consistency, allowing for a regression analysis to be conducted using their shared air temperature data.

As shown in Fig. 8, a regression analysis yields an R^2 of 0.99 and an RMSE of 0.89. Based on this relationship, ultrasonic anemometer data at corresponding time points were converted to match the AWS measurements, enabling the interpolation of missing temperature sensor values on AWS. The overall missing rate of the AWS temperature sensor was less than 1% and the interpolation records account for only a small portion of the complete extreme temperature dataset, which was subsequently used in the joint distribution analysis.

To verify the robustness of the imputation method, additional sensitivity tests were performed by randomly removing 3% and 5% of the AWS data. The remaining AWS data

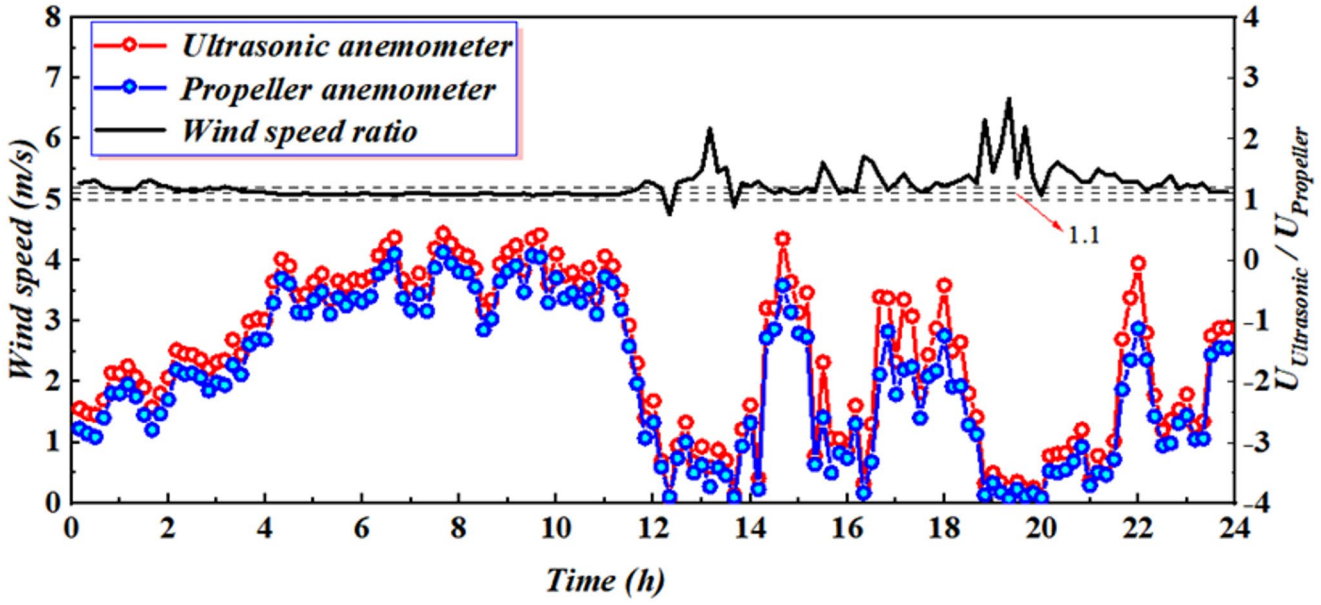

Fig. 7 Illustration of daily wind speed data

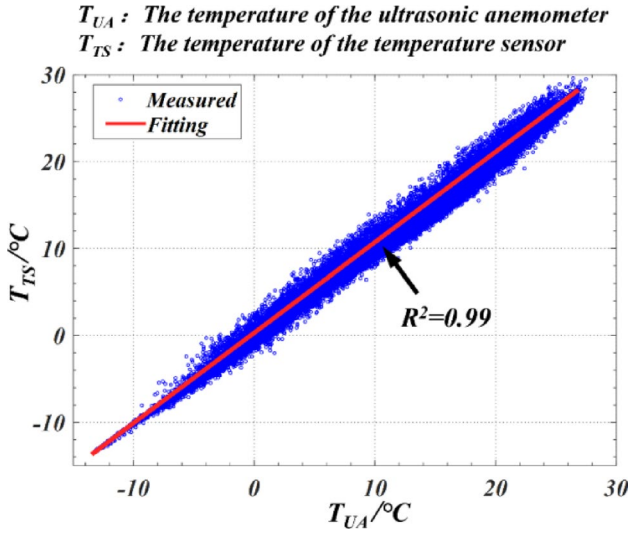

Fig. 8 Regression analysis of air temperature data

and the corresponding ultrasonic anemometer records were used to re-establish the regression model. The imputed values were then compared against the actual AWS observations, and the evaluation metrics (R^2 and RMSE) remained unchanged, indicating the deviations between imputed and actual values were negligible. These results confirm both the accuracy and stability of the proposed approach. The same interpolation method is also applied to wind speed. Since there is no solar radiation measurement data on the anemometer towers, the missing data are directly filled out using temporal interpolation methods (Dhevi 2014). The complete dataset after imputation provides a foundation for subsequent analysis.

Air temperature dominantly influences bridge temperature action values, most significantly impacting thermal expansion and contraction. The solar radiation and wind speed corresponding to extreme temperatures reflect the environmental effects most likely to accompany extreme temperature conditions, representing a climatic combination that significantly impacts the temperature effect values of the bridge. This study focuses exclusively on extreme air temperatures and their corresponding solar radiation and wind speed to ensure that the analysis results can directly contribute to evaluating the most unfavorable load combinations in bridge design. Future research may expand the data range to further validate and complement the current findings.

Due to the varying frequency and intensity of the combination occurrence of extreme air temperature, solar radiation, and wind speed during different observation periods, a single model is insufficient to capture the overall data distribution. Additionally, the aforementioned specification considers the effects of uniform temperature increase (hot season) and uniform temperature decrease (cold season) when evaluating the additional deformations in bridge structures caused by uniform temperature changes. Therefore, it is necessary to divide the data samples into hot and cold seasons.

As illustrated in Fig. 9, the hot and cold seasons are defined according to the variation patterns of daily extreme temperatures and the mean temperature. Specifically, the hot season is defined as the period spanning from May 1st to October 31st each year, while the cold season is defined as the period from November 1st to April 30th of the following year. This seasonal classification offers a structured foundation for analyzing and comparing temperature changes over distinct periods.

This study focuses on extreme environmental loads relevant to temperature actions on large-span bridges in complex mountainous areas. The samples of minimum air temperature and corresponding wind speed from the hot season and the samples of maximum air temperature and their corresponding solar radiation and wind speed samples from the cold season are disregarded due to their low application values for determining the temperature action values on large-span bridges in complex mountainous areas. The solar radiation corresponding to the minimum temperature is also excluded due to its weak correlation and small value. The distributions of extreme air temperatures and their corresponding solar radiation and wind speeds during hot and cold seasons are presented in Fig. 10.

It can be seen from Fig. 10 that the corresponding solar radiation and wind speed are much smaller than their extreme value when the air temperature reaches its extreme value in both hot and cold seasons. The extreme values of air temperature, solar radiation, and wind speed do not occur simultaneously, so it is necessary to establish joint distribution models of air temperature, solar radiation, and wind speed to explore their combined effects on large-span bridges in complex mountainous areas.

4 Results and discussion

4.1 Determination of marginal distributions of air temperature, solar radiation, and wind speed

The K–S test results (Table 3) confirm that the selected marginal distribution functions for environmental parameters are suitable, with all *p*-values exceeding 0.05 at a 0.05 significance level.

The fitting results (Fig. 11; Table 3) show that GEV, Gumbel, Weibull, and Logistic distributions perform well in modeling maximum temperatures in the hot season, with R^2 values up to 0.99 and RMSE less than 0.03. Although GEV shows the best fit, its complexity leads to selecting the

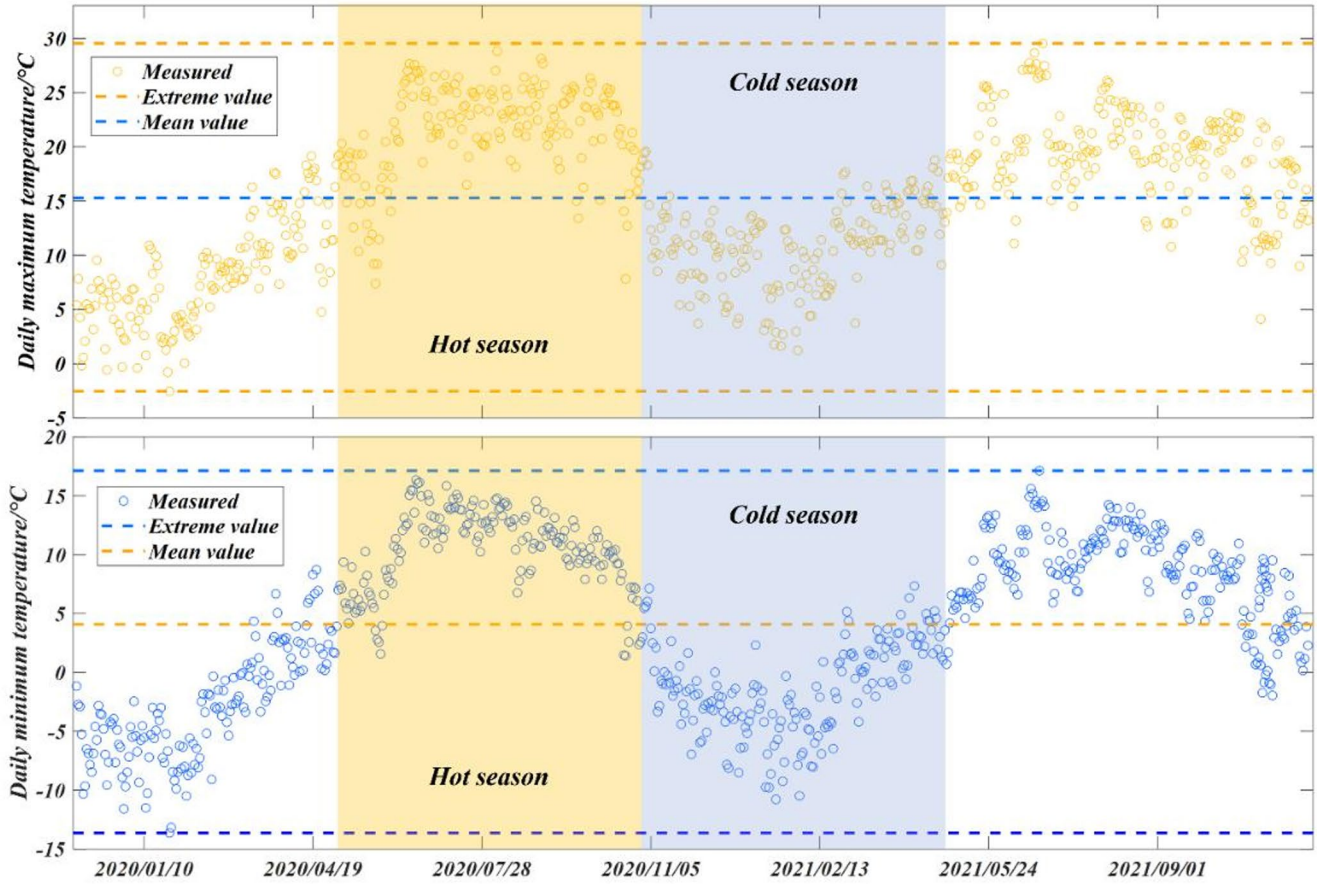

Fig. 9 The variation law of daily extreme temperatures

Weibull distribution, with a relatively lower BIC value, for maximum air temperature. Similarly, the Logistic distribution is chosen for solar radiation, and the Log-Normal distribution for wind speed, under hot seasons. The minimum temperature samples are predominantly negative values under the cold seasons, which precludes the use of distributions with strictly positive domains, such as the Log-Normal, Gamma, and Weibull distributions. In contrast, the Logistic distribution is well-suited for describing the distribution of minimum air temperatures, as it can accommodate negative values and provide a good fit to the data. On the other hand, the Gamma distribution is found to be an appropriate choice for characterizing the wind speed distribution corresponding to the minimum air temperature, due to its ability to model skewed and non-negative distributions (Table 3).

4.2 Joint distributions of air temperature, solar radiation, and wind speed

After selecting the optimal distribution functions for the environmental parameters, the optimal joint distribution of air temperature, solar radiation, and wind speed under both cold and hot seasons is established by choosing different Copula functions.

4.2.1 Joint distribution of air temperature, solar radiation, and wind speed during the hot season

Through Eq. (1), the Kendall rank correlation coefficients between maximum air temperature and its corresponding solar radiation and wind speed are 0.38 and 0.25, respectively. This indicates a predominantly positive correlation during hot seasons, with a stronger relationship between maximum air temperature and solar radiation compared to wind speed. Through Eq. (1) to Eq. (5), the parameters of the bivariate Copula models for the maximum air temperature and its corresponding solar radiation and wind speed in the hot season can be calculated, with results shown in Table 4.

The fitting results of the bivariate joint distributions of the maximum air temperature and its corresponding solar radiation and wind speed established using different Copulas are shown in Figs. 12 and 13, and Table 5.

Based on goodness-of-fit metrics in Table 5, the Clayton model is the best fit for the joint distributions of maximum

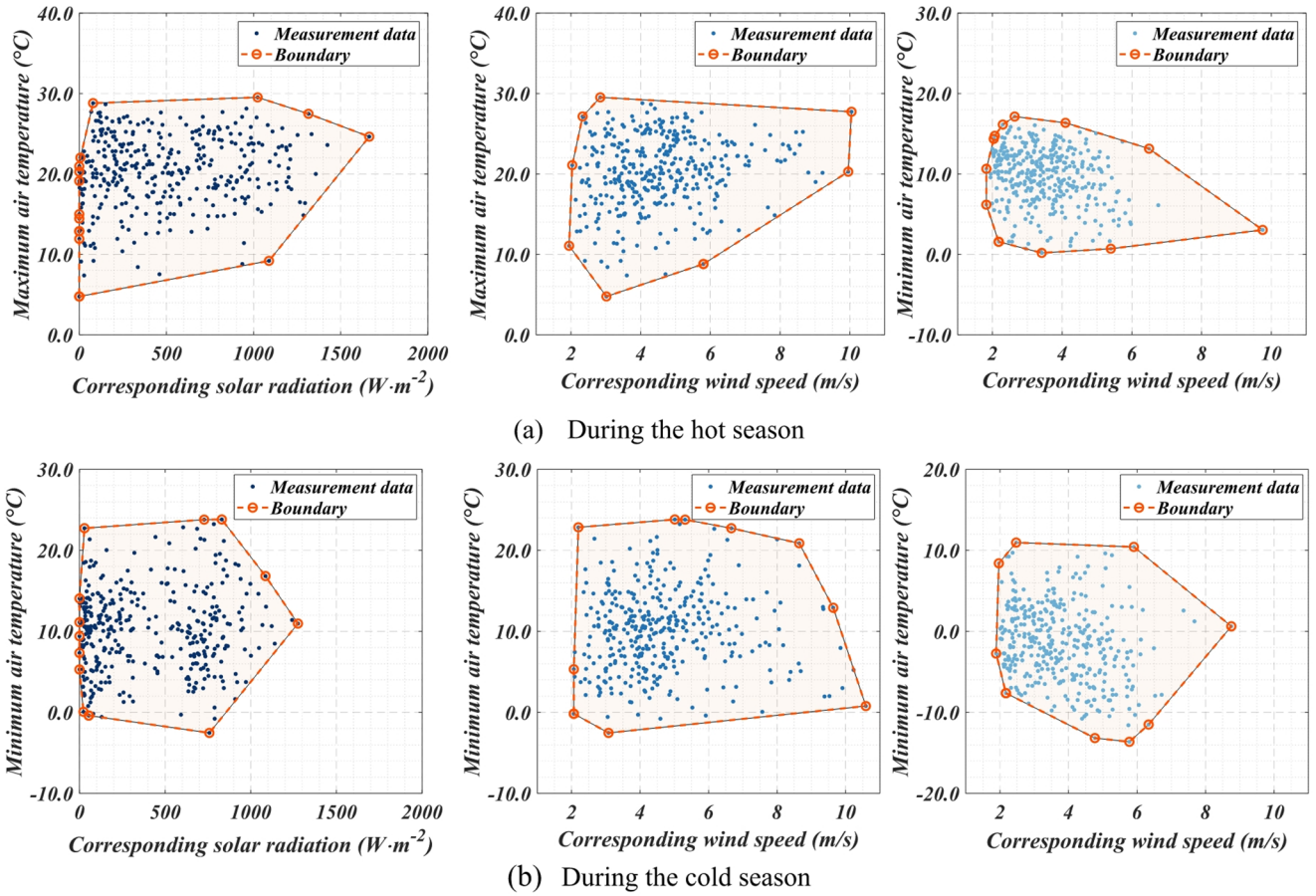

Fig. 10 Distribution of extreme air temperatures and their corresponding solar radiation and wind speed

air temperature with solar radiation and wind speed. In subsequent analysis, a trivariate joint distribution of maximum air temperature, solar radiation, and wind speed is constructed. Using the MLE method, the parameters for the Clayton, Frank, and Gumbel models are estimated as 0.19, 0.69, and 1.06, respectively. The fitting results of the trivariate joint distributions using different Copulas are presented in Table 6; Fig. 14.

According to Table 6, the Clayton Copula shows the best fit for the distribution of the maximum air temperature and its corresponding solar radiation and wind speed, with R^2, RMSE, and BIC values of 0.983, 0.028, and −2589, respectively.

4.2.2 Joint distribution of air temperature and wind speed during the cold season

The Kendall rank correlation coefficient between maximum temperature and corresponding wind speed is −0.17, indicating a negative relationship under cold season conditions. The Clayton, Frank, and Gumbel Copula models yielded parameters of 0.01, −1.47, and 1.00, respectively. As shown in Fig. 15, the Frank Copula provides the best fit to the joint distribution of minimum air temperature and wind speed, with R^2 = 0.988, RMSE = 0.023, and BIC = −2758.

4.3 The joint values of air temperature, solar radiation, and wind speed under return periods

In this section, a multi-parameter optimal joint distribution model is employed to estimate the joint values under multivariate return periods. These joint values are then compared with the univariate extreme values corresponding to the same return periods to highlight the differences. The statistics of environmental parameter extremes under univariate return periods are presented in Sect. 4.3.1.

4.3.1 Extreme values of air temperature and its corresponding solar radiation/wind speed under the univariate return period

The extreme values of air temperature and its corresponding solar radiation and wind speed under the univariate return period are shown in Fig. 16. It can be seen from Fig. 16 that during the hot season, the extreme value of the maximum temperature is 38.1 °C, the extreme solar radiation is

Table 3 Fitting results of environmental parameters

Parameter classification	Environmental parameter	Distribution type	K–S	Parameters			Evaluation index		
				μ	σ	k	R^2	RMSE	BIC
During the hot seasons	The maximum air temperature	GEV	0.71	−0.44	4.72	19.17	0.998	0.012	−3184
		Log-Normal	0.75	2.99	0.25	–	0.964	0.055	−2095
		Gamma	0.36	–	17.87	1.14	0.978	0.043	−2265
		Gumbel	0.76	22.49	3.76	–	0.993	0.025	−2677
		Weibull	**0.62**	**22.11**	**5.52**	**–**	**0.997**	**0.015**	**−3057**
		Logistic	0.44	20.61	2.52	–	0.996	0.019	−2880
	The solar radiation corresponds to the maximum air temperature	GEV	0.70	0.07	287.29	303.65	0.976	0.044	−2221
		Gumbel	0.76	684.61	389.84	–	0.945	0.067	−1929
		Logistic	0.63	**464.01**	**222.07**	**–**	**0.970**	**0.049**	**−2150**
	The wind speed corresponds to the maximum air temperature	GEV	0.32	−0.02	1.20	3.87	0.998	0.013	−3161
		Log-Normal	**0.72**	**1.46**	**0.32**	**–**	**0.998**	**0.012**	**−3221**
		Gamma	0.77	–	9.85	0.46	0.998	0.012	−3175
		Gumbel	0.64	5.34	1.78	–	0.917	0.083	−1794
		Weibull	0.68	5.07	3.17	–	0.983	0.037	−2376
		Logistic	0.50	4.43	0.82	–	0.995	0.020	−2832
During the cold seasons	The minimum air temperature	GEV	0.43	−0.24	4.56	−3.27	0.999	0.008	−3462
		Gumbel	0.47	0.82	4.69	–	0.977	0.044	−2270
		Logistic	0.53	**−1.59**	**2.70**	**–**	**0.997**	**0.016**	**−3022**
	The wind speed corresponds to the minimum air temperature	GEV	0.35	−0.04	0.99	3.23	0.987	0.033	−2471
		Log-Normal	0.46	1.28	0.32	–	0.988	0.032	−2497
		Gamma	**0.40**	**–**	**10.25**	**0.37**	**0.989**	**0.030**	**−2539**
		Gumbel	0.61	4.39	1.36	–	0.953	0.062	−2008
		Weibull	0.45	4.20	3.36	–	0.988	0.032	−2500
		Logistic	0.41	3.70	0.69	–	0.984	0.036	−2406

The bolded data indicate the selected marginal distribution for the corresponding environmental parameter.μ represents the location parameter, σ represents the scale parameter, and k represents the shape parameter

2840 W/m^2, and the extreme wind speed is 33 m/s under the 100-year return period. During the cold season, the extreme value of the minimum temperature is −20.3 °C, and the extreme wind speed is 34.9 m/s under the 100-year return period. It can be observed that directly superimposing these environmental loads during bridge design would significantly overestimate the bridge design loads. Based on Sect. 2.4.3, the joint values of temperature, solar radiation, and wind speed during different seasons are calculated as follows.

4.3.2 The joint values of air temperature, solar radiation, and wind speed during the hot season

(1) Bivariate joint distribution

During the hot seasons, the contour maps of the bivariate joint distribution of maximum air temperature and its corresponding solar radiation and wind speed under different return periods are shown in Fig. 17, and the corresponding joint values are shown in Table 7.

As shown in Fig. 17a; Table 7, the joint values of maximum temperature and solar radiation under the Kendall return period increase with return periods. The growth rates of both parameters decrease over time. Notably, univariate return periods yield significantly higher extreme values for maximum air temperature, solar radiation, and wind speed compared to bivariate joint distributions. A similar pattern is observed for the joint values of maximum temperature and wind speed (Fig. 17b; Table 7). Considering multivariate joint distributions provides a more realistic assessment of risk, avoiding overestimations and highlighting the importance of accounting for multiple environmental factors in long-term engineering projects.

Under the bivariate return periods, the maximum air temperature values in the joint values under the "OR" return period are usually the highest, followed by the Kendall return period, and the lowest for the "AND" return period. This analysis validates that joint extreme air temperature values derived from the "OR" return period tend to yield overly conservative designs, potentially leading to unnecessary costs and excessive safety margins. Conversely, those based on the "AND" return period may result in unsafe design conditions, compromising the structural integrity and reliability of the bridge. Therefore, it is recommended to adopt a more balanced approach by selecting the maximum air temperature value from the bivariate joint values

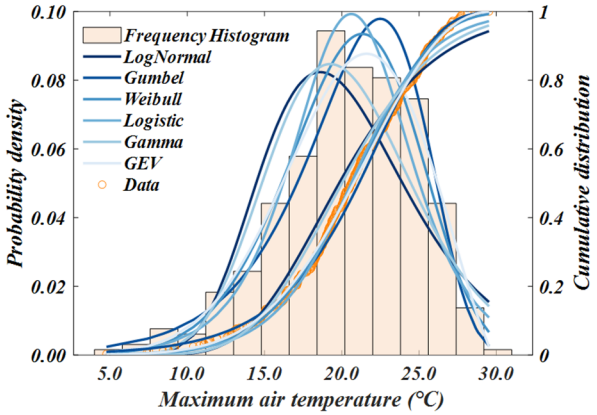

(a) The maximum air temperature

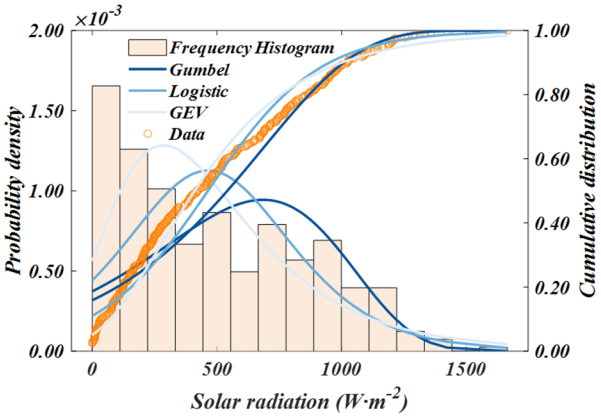

(b) The solar radiation corresponding to the maximum air temperature

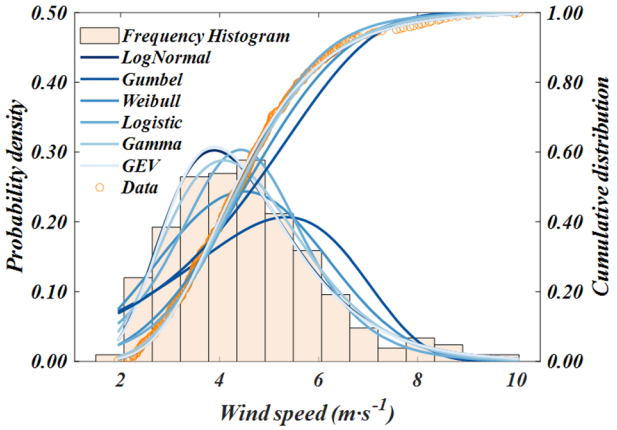

(c) The wind speed corresponds to the maximum air temperature

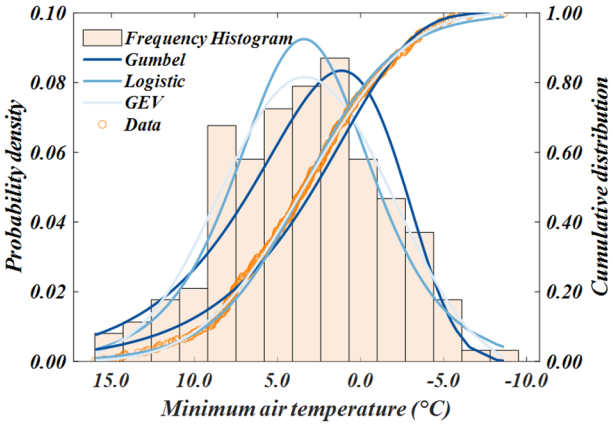

(d) The minimum air temperature

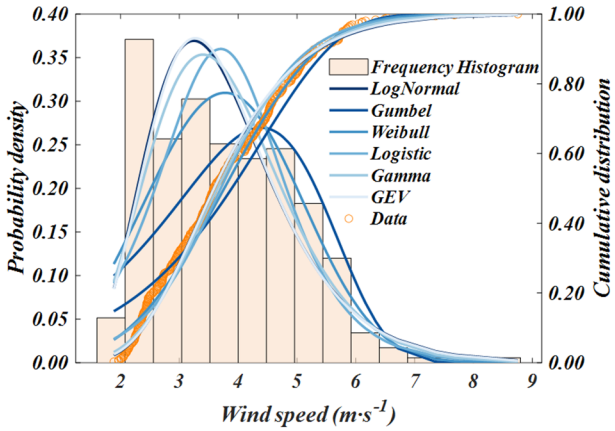

(e) The wind speed corresponds to the minimum air temperature

Fig. 11 The marginal distribution fitting of air temperature, solar radiation, and wind speed. **a**–**c** During the hot season; **d** and **e** During the cold season

under the Kendall return period as the basis for determining the design value of the bridge's maximum air temperature. This approach provides a more accurate and reliable estimate of extreme air temperature values.

(2) Trivariate joint distribution

For the trivariate joint distribution of maximum temperature, solar radiation, and wind speed, the Clayton Copula model is selected for its superior regression performance.

Table 4 The parameters of the copula functions for different environmental parameters

Copula functions	Joint distributions of maximum air temperature and its corresponding solar radiation during the hot season	Joint distributions of maximum air temperature and its corresponding wind speed during the hot season
Clayton	0.18	0.20
Frank	0.60	0.91
Gumbel	1.06	1.06

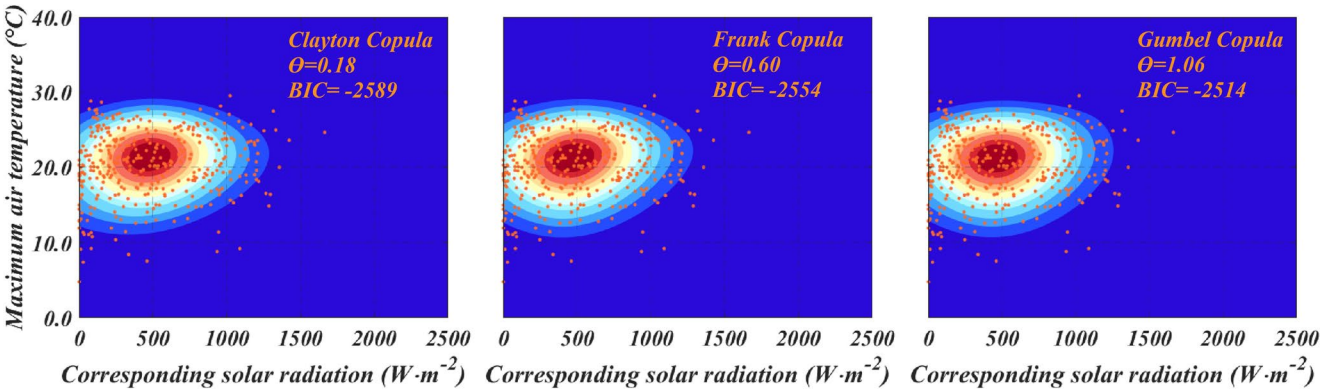

Fig. 12 The PDF of the bivariate joint distribution of the maximum air temperature and corresponding solar radiation

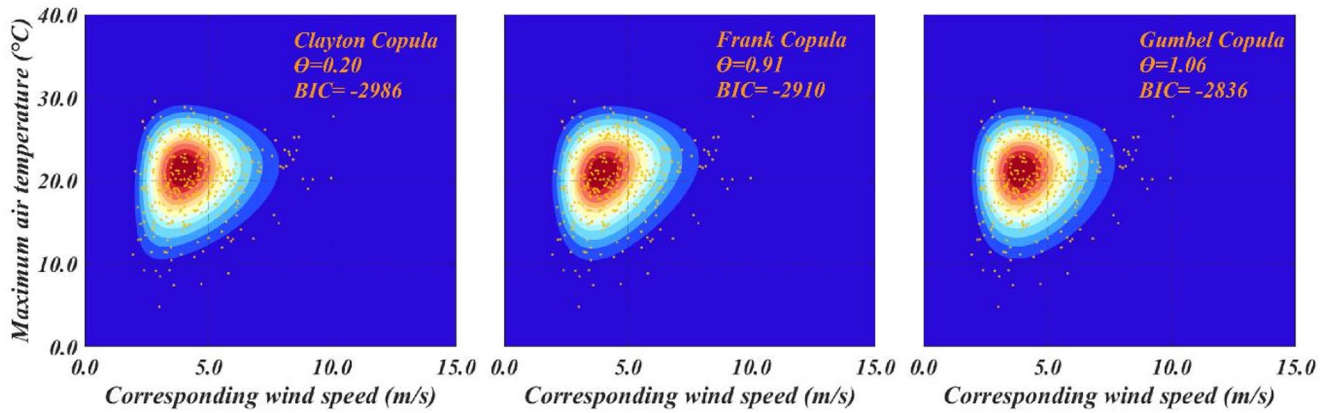

Fig. 13 The PDF of the bivariate joint distribution of the maximum air temperature and corresponding wind speed

Table 5 Fitting results of the bivariate joint distribution of the maximum air temperature and its corresponding solar radiation, and wind speed

Bivariate distributions	Copula functions	Evaluation index		
		R^2	RMSE	BIC
The maximum air temperature and corresponding solar radiation	Clayton	0.983	0.028	−2589
	Frank	0.982	0.030	−2554
	Gumbel	0.980	0.031	−2514
The maximum air temperature and corresponding wind speed	Clayton	0.994	0.016	−2986
	Frank	0.993	0.018	−2910
	Gumbel	0.991	0.020	−2836

Blackened data is the selected bivariate joint distribution

Table 6 Fitting results of the trivariate joint distribution of the maximum air temperature and its corresponding solar radiation/wind speed during the hot season

Copula functions	Evaluation index		
	R^2	RMSE	BIC
Clayton	0.985	0.019	−2882
Frank	0.980	0.022	−2780
Gumbel	0.976	0.024	−2711

Blackened data is the selected bivariate joint distribution

The joint values for different return periods (10, 20, 30, 50, and 100 years) are presented in Table 8 and visualized in Fig. 18.

From Table 8, the Kendall return period yields joint values that fall between those of the "OR" and "AND" return periods. For the same return year, the trivariate return period results in lower maximum air temperature values compared

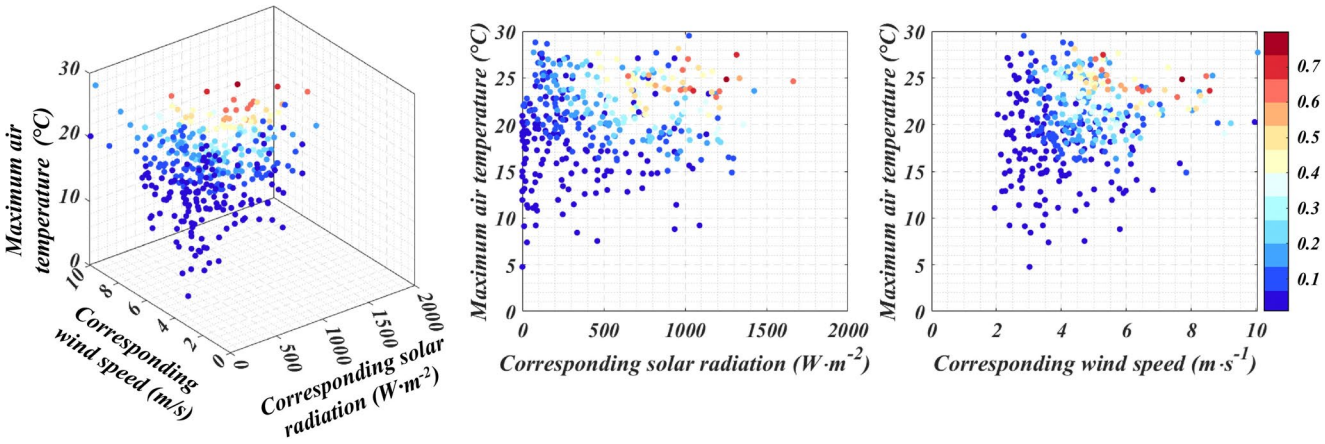

Fig. 14 The trivariate Clayton Copula model for maximum air temperature and its corresponding solar radiation and wind speed in the hot season

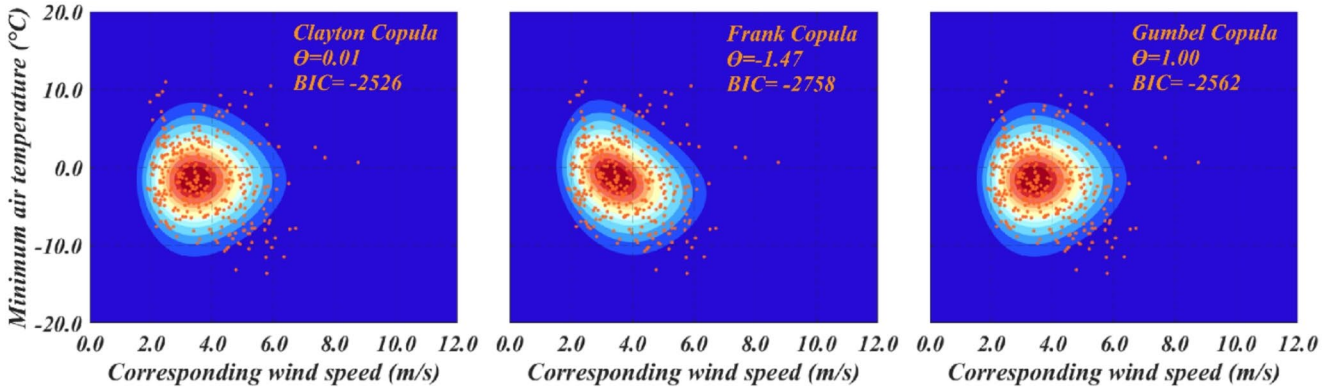

Fig. 15 The PDF of the bivariate joint distribution of the minimum air temperature and corresponding wind speed

to univariate and bivariate return periods. The "OR" return period consistently produces the highest joint values, followed by the Kendall return period, with the "AND" return period yielding the lowest values. Moreover, as the return period increases, the growth rate of joint values under all return periods slows down. Based on this analysis, the maximum air temperature under the Kendall return period is recommended for analyzing design values for the maximum bridge temperature.

4.3.3 The joint values of the minimum air temperature and corresponding wind speed during the cold season

During the cold seasons, the contour map of the joint distribution of minimum air temperature and corresponding wind speed under different return periods is shown in Fig. 19, and the corresponding joint values are shown in Table 9.

Figure 19; Table 9 indicate that the minimum air temperature values in the joint values under the Kendall return period fall between those of the "OR" return period and the "AND" return period. As the return period increases, the minimum temperature gradually decreases while the corresponding wind speed gradually increases, and the growth rates of both parameters gradually decrease. For the same return year, the absolute values of the minimum air temperature and wind speed under the univariate return period are greater than the joint values under the bivariate return period. The joint values of the minimum air temperature under the Kendall return period can be selected for the design value of the bridge's minimum temperature.

4.4 Temperature action values of Bridge structures

After obtaining the joint values of air temperature and its corresponding solar radiation and wind speed for different return periods, the temperature action values on the bridge structure for different return periods can be calculated according to Sect. 2.5. The classification by seasonal conditions is as follows.

4.4.1 Maximum temperature action value

Under hot season conditions, the maximum air temperature values in the joint values calculated from different joint

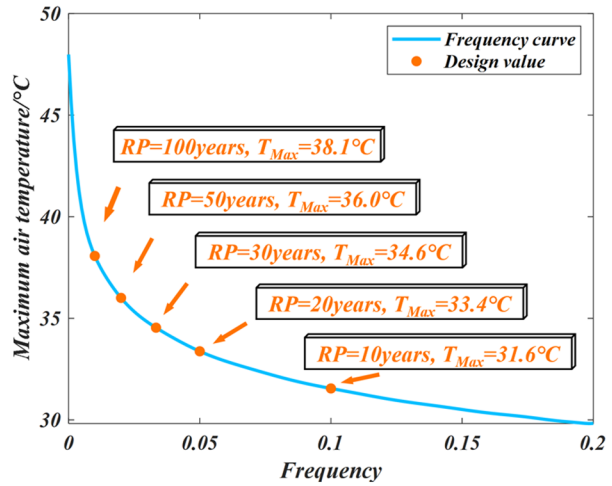

(a) Maximum air temperature

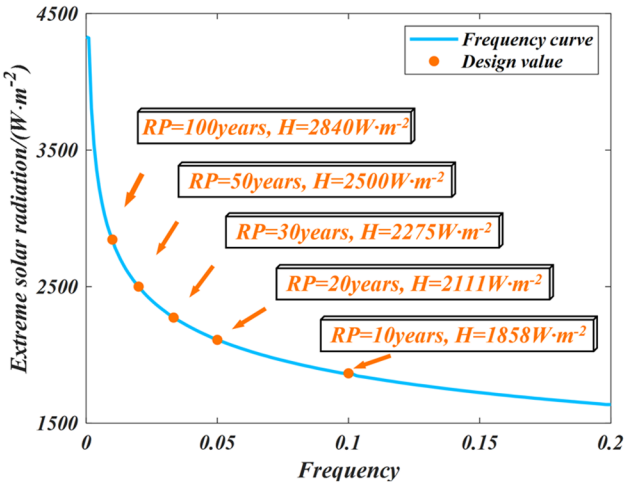

(b) Extreme solar radiation

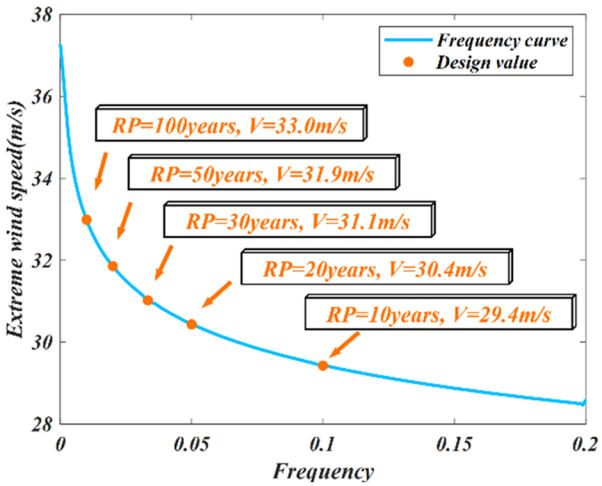

(c) Extreme wind speed

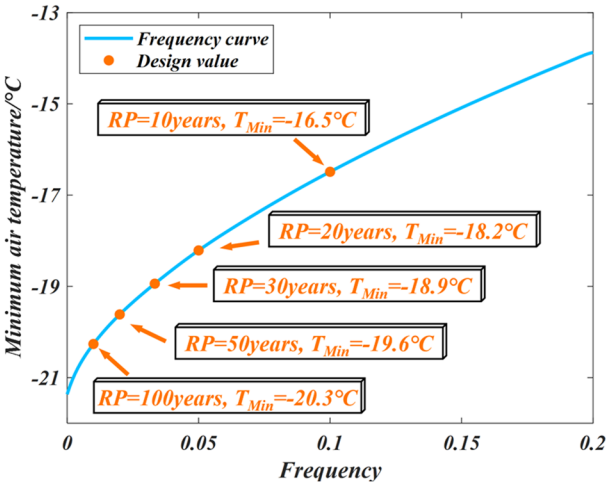

(d) Minimum air temperature

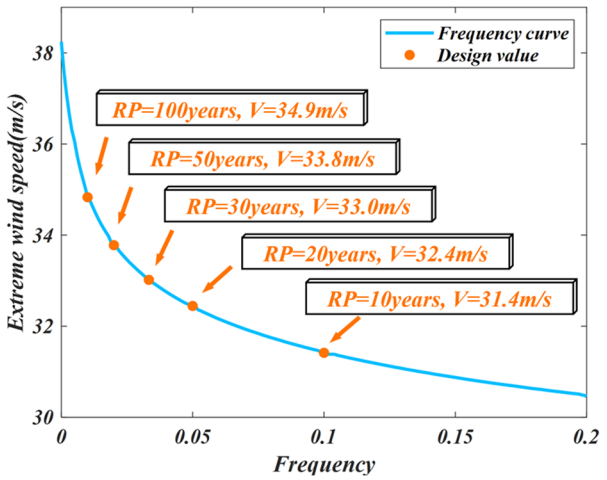

(e) Extreme wind speed

Fig. 16 The extreme values of air temperature, solar radiation, and wind speed under the univariate return period. **a**–**c** During the hot season; **d**, **e** During the cold season

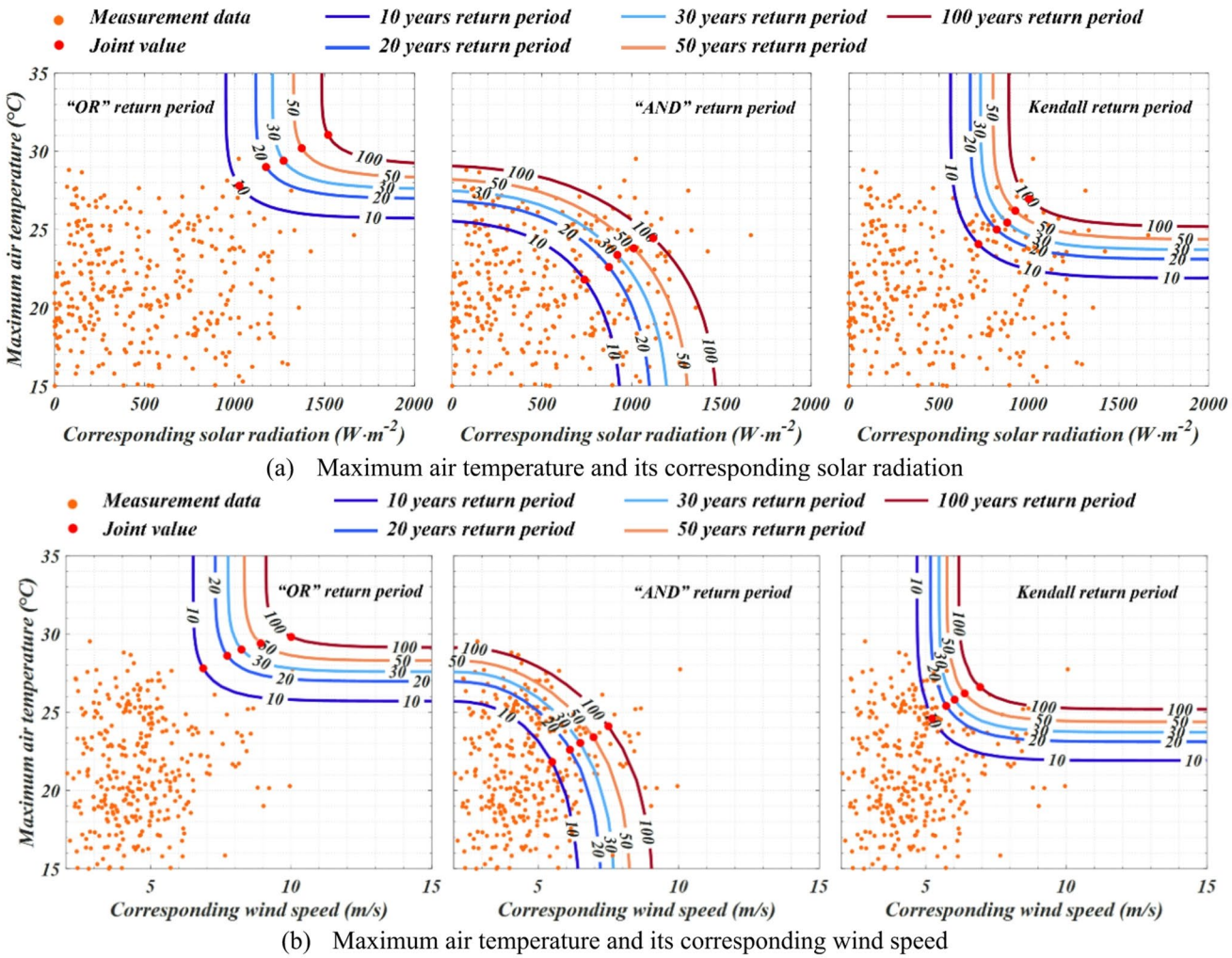

Fig. 17 The contour map of the bivariate joint distribution of maximum air temperature and its corresponding solar radiation and wind speed under different return periods during the hot season (Clayton)

Table 7 The bivariate joint values of maximum air temperature and its corresponding solar radiation and wind speed under different return periods during the hot season (Clayton)

Bivariate distributions	Return years	"OR" return period		"AND" return period		The Kendall return period	
		Maximum air temperature	Solar radiation	Maximum air temperature	Solar radiation	Maximum air temperature	Solar radiation
The maximum air temperature and corresponding solar radiation	10-year	27.8	1026	21.0	783	24.1	720
	20-year	29.0	1175	21.9	920	25.0	822
	30-year	29.4	1273	22.2	1000	25.4	880
	50-year	30.2	1373	22.9	1080	26.2	925
	100-year	31.1	1520	23.4	1206	27.0	1000
Bivariate distributions	Return years	"OR" return period		"AND" return period		The Kendall return period	
		Maximum air temperature	Wind speed	Maximum air temperature	Wind speed	Maximum air temperature	Wind speed
The maximum air temperature and corresponding wind speed	10-year	27.8	6.9	21.8	5.5	24.6	5.2
	20-year	28.6	7.7	22.6	6.1	25.4	5.7
	30-year	29.0	8.2	23.0	6.5	25.8	6.0
	50-year	29.4	8.9	23.4	7.0	26.2	6.4
	100-year	29.8	10.0	24.1	7.5	26.6	6.9

The unit of Solar radiation is W/m^2, the unit of wind speed is m/s, and the unit of maximum air temperature is °C

Table 8 The trivariate joint values of maximum air temperature and its corresponding solar radiation and wind speed under different return periods during the hot season (Clayton)

Return years	"OR" return period			"AND" return period			The Kendall return period		
	Maximum air temperature	Solar radiation	Wind speed	Maximum air temperature	Solar radiation	Wind speed	Maximum air temperature	Solar radiation	Wind speed
10-year	23.3	700	6.5	18.5	452	3.0	22.5	500	5.5
20-year	25.1	800	7.0	18.9	535	3.1	23.0	600	6.0
30-year	26.0	900	7.0	19.5	596	3.2	23.6	650	6.0
50-year	27.0	991	7.5	20.0	683	3.3	24.2	700	6.5
100-year	28.0	1073	8.5	20.5	799	3.5	24.8	750	6.5

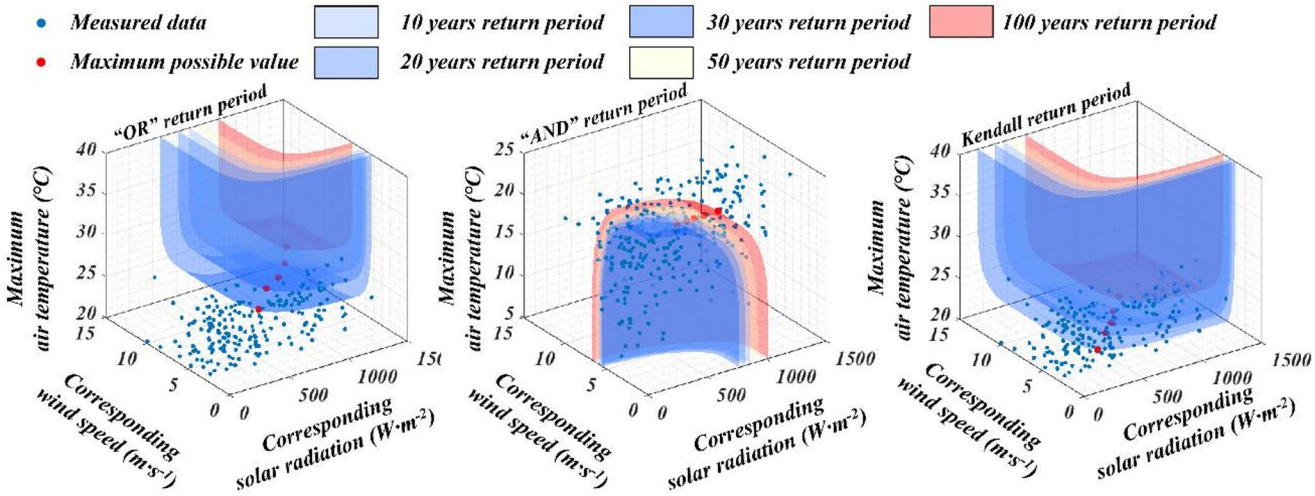

Fig. 18 The contour map of the trivariate joint distribution of maximum air temperature and its corresponding solar radiation and wind speed under different return periods during the hot season (Clayton)

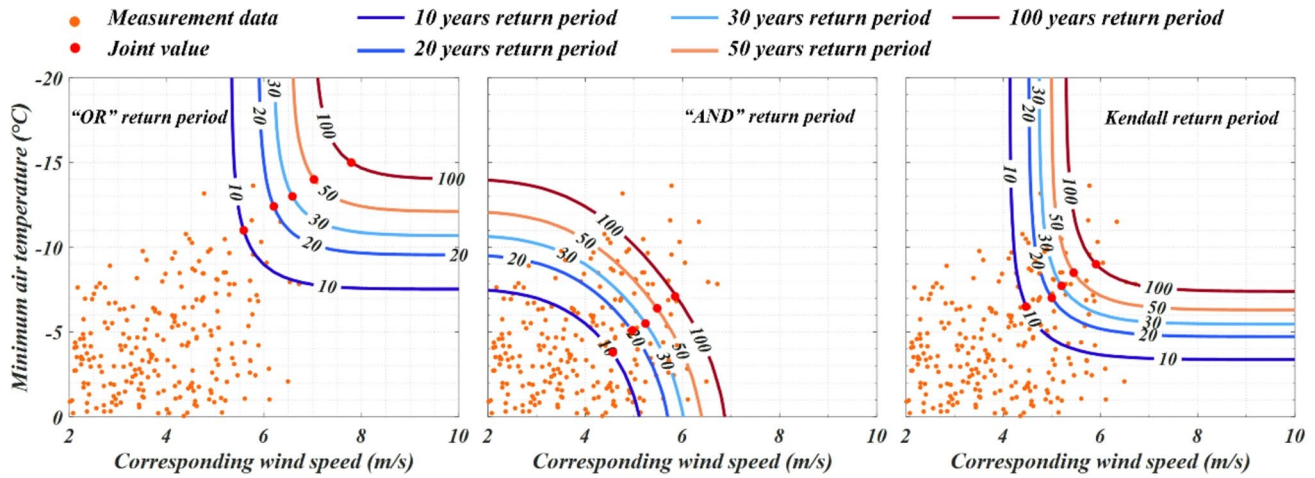

Fig. 19 The contour map of the bivariate joint distribution of minimum air temperature and corresponding wind speed under different return periods during the cold season (Frank)

distributions under the different return periods are converted into temperature action values for three different bridge structures, as shown in Table 10.

As shown in Table 10, for the different bridge structures under the Kendall return period, the maximum temperature action values are the smallest when considering the influence of the trivariate joint distribution, followed by those under the bivariate joint distribution, while the maximum temperature action values obtained under the univariate return period are the largest. The multivariate joint distribution accounts for the synergistic effects among environmental parameters, thereby more accurately reflecting the joint probabilities of

Table 9 The bivariate joint values of minimum air temperature and its corresponding wind speed under different return periods during the cold season (Frank)

Return years	"OR" return period		"AND" return period		The Kendall return period	
	Minimum air temperature	Wind speed	Minimum air temperature	Wind speed	Minimum air temperature	Wind speed
10-year	−11.0	5.6	−3.8	4.6	−6.5	4.5
20-year	−12.4	6.2	−5.1	5.0	−7.0	5.0
30-year	−13.0	6.6	−5.5	5.2	−7.7	5.2
50-year	−14.0	7.0	−6.4	5.5	−8.5	5.4
100-year	−15.0	7.8	−7.1	5.8	−9.0	5.9

The unit of wind speed is m/s, and the unit of maximum air temperature is °C

Table 10 The maximum temperature action values of Bridge structures (unit: °C)

Joint distributions	Return Periods	Return years	Air temperature values	Steel bridges with steel deck slab	Steel bridges with concrete deck slab	Concrete bridges, stone bridges
	Univariate	10-year	31.6	43.8	36.3	32.4
		20-year	33.4	44.7	37.5	33.7
		30-year	34.6	45.3	38.4	34.6
		50-year	36.0	46.0	39.3	35.6
		100-year	38.1	47.1	40.8	37.1
The bivariate joint distributions of maximum air temperature and corresponding solar radiation	Kendall	10-year	24.1	40.1	31.1	27.1
		20-year	25.0	40.5	31.7	27.7
		30-year	25.4	40.7	32.0	28.0
		50-year	26.2	41.1	32.5	28.6
		100-year	27.0	41.5	33.1	29.1
The bivariate joint distributions of maximum air temperature and corresponding wind speed	Kendall	10-year	24.6	40.3	31.4	27.4
		20-year	25.4	40.7	32.0	28.0
		30-year	25.8	40.9	32.3	28.3
		50-year	26.2	41.1	32.5	28.6
		100-year	26.6	41.3	32.8	28.9
The trivariate joint distributions of maximum air temperature and its corresponding solar radiation/ wind speed	Kendall	10-year	20.1	38.1	28.3	24.2
		20-year	21.3	38.7	29.1	25.1
		30-year	22.4	39.2	29.9	25.9
		50-year	23.3	39.7	30.5	26.5
		100-year	24.8	40.4	31.6	27.6

extreme events. This approach avoids the overestimation of loads caused by the independence assumption in univariate analysis, making it more aligned with the practical design requirements for bridges in complex mountainous areas. To investigate the changes in the maximum temperature action values for bridge structures under multivariate return periods, the reduction coefficients for the maximum temperature action of different bridge structures through Eq. (14) are shown in Table 11.

As presented in Table 11, for a given return year, the reduction coefficients of maximum temperature action for various bridge types under the same joint distribution are identical. This consistency can be attributed to the linear nature of the temperature load equations specified in bridge design codes for different structural types. When calculating the reduction factor, the result is solely dependent on the air temperature values corresponding to different return years. In defining the reduction factor, we considered the limitation that directly comparing temperatures (T_D/T_M) may result in unreliable values when the temperature approaches 0 °C, potentially failing to capture actual thermal variations accurately. Therefore, we defined the temperature action reduction factor as the ratio of the difference between the extreme temperature under different return periods and the mean temperature of the univariate return period. This definition effectively quantifies the reduction in thermal effects by capturing the fluctuation range of the extreme temperature relative to a baseline. Furthermore, validation using three representative bridge types confirmed that the proposed temperature action reduction factor accurately reflects the reduction in ambient temperature variation, thereby substantiating the universality of the proposed definition approach. Under the bivariate return period, as the return period increases, the temperature reduction coefficients for the three types of bridge structures under the joint distribution of maximum temperature and corresponding wind speed gradually decrease from 0.56 to

Table 11 Reduction coefficients of the maximum temperature action

Joint distributions	Return years	Steel bridges with steel deck slab	Steel bridges with concrete deck slab	concrete bridges, stone bridges
The bivariate joint distributions of maximum air temperature and corresponding solar radiation	10-year	0.53	0.53	0.53
	20-year	0.53	0.53	0.53
	30-year	0.51	0.51	0.51
	50-year	0.50	0.50	0.50
	100-year	0.48	0.48	0.48
The bivariate joint distributions of maximum air temperature and corresponding wind speed	10-year	0.56	0.56	0.56
	20-year	0.55	0.55	0.55
	30-year	0.53	0.53	0.53
	50-year	0.50	0.50	0.50
	100-year	0.46	0.46	0.46
The trivariate joint distributions of maximum air temperature and its corresponding solar radiation/wind speed	10-year	0.43	0.43	0.43
	20-year	0.41	0.41	0.41
	30-year	0.41	0.41	0.41
	50-year	0.40	0.40	0.40
	100-year	0.37	0.37	0.37

0.46. This change is more pronounced than that observed for the joint distribution of maximum temperature and corresponding solar radiation, indicating that the relationship between maximum air temperature and wind speed is gradually tightened, and the degree of interaction increases as the return period increases. Under the trivariate joint distribution, as the return year increases, the reduction coefficients for the three types of bridge structures gradually decrease from 0.43 to 0.37, which are smaller than those under the bivariate joint distribution. This indicates that the more environmental parameters considered, the more pronounced the reduction effect on the maximum temperature action for bridge structures.

Table 13 Reduction coefficients of the minimum temperature action

Return years	Steel bridges with steel deck slab	Steel bridges with concrete deck slab	Concrete bridges, stone bridges
10 years	0.53	0.53	0.53
20 years	0.53	0.53	0.53
30 years	0.52	0.52	0.52
50 years	0.51	0.51	0.51
100 years	0.49	0.49	0.49

4.4.2 Minimum temperature action value

Under cold season conditions, the minimum temperature action values of bridge structures under different return periods are shown in Table 12.

As shown in Table 12, the minimum temperature action values under the Kendall return period are significantly greater than those obtained under the univariate return period. The reduction coefficients for the minimum temperature action of different bridge structures are shown in Table 13.

As shown in Table 13, with the increase of the return years, the reduction coefficients of the three types of bridge structures gradually decreased from 0.53 to 0.49, indicating a strong correlation between minimum temperature and wind speed as the return years increase and a significant reduction effect of minimum temperature action. The calculated reduction coefficients can provide a reference for selecting the most unfavorable design temperature parameters for mountain bridges.

Table 12 The minimum temperature action values of Bridge structures (unit: °C)

Joint distributions	Return Period	Return years	Temperature value	Steel bridges with steel deck slab	Steel bridges with concrete deck slab	Concrete bridges, stone bridges
	Univariate	10 years	−16.5	−19.6	−13.8	−9.3
		20 years	−18.2	−21.5	−15.2	−10.3
		30 years	−18.9	−22.2	−15.7	−10.8
		50 years	−19.6	−23.0	−16.3	−11.2
		100 years	−20.3	−23.8	−16.9	−11.7
The bivariate joint distributions of maximum air temperature and corresponding wind speed	Kendall	10 years	−6.5	−8.6	−5.5	−2.9
		20 years	−7.0	−9.2	−5.9	−3.3
		30 years	−7.7	−9.9	−6.5	−3.7
		50 years	−8.5	−10.8	−7.1	−4.2
		100 years	−9.0	−11.4	−7.6	−4.5

5 Conclusions

This study employs different Copula functions to establish the joint distribution models of air temperature, solar radiation, and wind speed based on field-measured environmental parameter data from complex mountainous bridge sites. It deduces the joint values under different return periods, which are subsequently converted to extreme temperature action values for the design of bridge structures. A reduction coefficient of temperature action is proposed to reflect the differences in temperature action values between univariate and multivariable return periods. The main conclusions are summarized as follows:

(1) Dividing environmental parameters into cold and hot seasons overcomes the limitation of a single model in capturing distribution characteristics across the entire observation period, and is consistent with bridge design specifications that categorize temperature actions as uniform temperature increases or decreases.
(2) Observations at the study's bridge site reveal that extreme air temperature events rarely coincide with concurrent extremes in solar radiation and wind speed.
(3) The optimal marginal distributions for extreme environmental parameters are: Weibull for maximum temperature, Logistic for hot season solar radiation and minimum temperature, Log-Normal for hot season wind speed, and Gamma for cold season wind speed.
(4) The maximum air temperature has a positive correlation with its corresponding solar radiation and wind speed, best modeled by the Clayton Copula. In contrast, the minimum air temperature has a negative correlation with wind speed, which is effectively captured by the Frank Copula.
(5) The absolute values of joint values under multivariate return periods are lower than those of corresponding extremes under univariate return periods. For bridge temperature actions, the joint values of air temperature and its corresponding solar radiation and wind speed under the Kendall return period provide more realistic estimates compared to univariate approaches.
(6) The temperature reduction coefficients under the trivariate joint distribution are smaller than those under the bivariate joint distribution, indicating that the more environmental parameters considered, the more pronounced the reduction effect on the temperature action for bridge structures.

Supplementary Information The online version contains supplementary material available at https://doi.org/10.1007/s00477-025-03114-w.

Acknowledgements The support from the National Natural Science Foundation of China (No.52278533); Natural Science Foundation of Sichuan Province (No.2023NSFSC1961).

Author contributions Mingjin Zhang: Conceptualization, Project Administration, Resources, Methodology, Jiale Long: Software, Formal Analysis, Writing - Original Draft, Jingxi Qin: Validation, Investigation, Writing – Original Draft, Review & Editing, Jinxiang Zhang: Validation, Investigation, Xulei Jiang: Validation, Investigation, Yongle Li: Supervision, Funding acquisition.

Funding Open access funding provided by The Hong Kong Polytechnic University

Data availability No datasets were generated or analysed during the current study.

Declarations

Conflict of interest The authors declare no competing interests.

References

Abid SR, Tayşi N, Özakça M (2016) Experimental analysis of temperature gradients in concrete box-girders. Constr Build Mater 106:523–532. https://doi.org/10.1016/j.conbuildmat.2015.12.144

Abid SRR, Xue J, Liu J et al (2022) Keywords: concrete box-girder temperature gradient Bridge mean temperature solar radiation. Structures 37:960–976. https://doi.org/10.1016/j.istruc.2022.01.070

Abraj Ma, Hewaarachchi M AP (2021) Joint return period Estimation of daily maximum and minimum temperatures using copula method. Adv Appl Stat 66:175–190. https://doi.org/10.17654/AS066020175

American Association of State Highway and Transportation Officials (2020) LRFD bridge design specifications, 9th edition. Washington, DC

Casella G, Berger R (2024) Statistical inference. CRC

Chen B, Guo WH, Song CF, Lu KK (2012) Numerical assessment on time-varying temperature field of bridge tower under solar radiation. Appl Mech Mater 204–208:2236–2239. https://doi.org/10.4028/www.scientific.net/AMM.204-208.2236

Chen Q, Yu C, Li Y (2022) General strategies for modeling joint probability density function of wind speed, wind direction and wind attack angle. J Wind Eng Ind Aerodyn 225:104985. https://doi.org/10.1016/j.jweia.2022.104985

de Kampé J (1973) Mesure de l'information par un ensemble d'observateurs indépendants. pp 315–329

Dhevi ATS (2014) Imputing missing values using Inverse Distance Weighted Interpolation for time seriesdata. In: 2014 Sixth International Conference on Advanced Computing (ICoAC). pp 255–259. https://doi.org/10.1109/ICoAC.2014.7229721

Dilger WH, Ghali A, Chan M et al (1983) Temperature Stresses in Composite Box Girder Bridges. J Struct Eng 109:1460–1478. https://doi.org/10.1061/(ASCE)0733-9445

Emerson M (1976) Bridge temperatures estimated from the shade temperature

European Committee for Standardization (2004) Eurocode 1: actions on structures. Belgium

Fenerci A, Øiseth O, Rønnquist A (2017) Long-term monitoring of wind field characteristics and dynamic response of a long-span suspension Bridge in complex terrain. Eng Struct 147:269–284. https://doi.org/10.1016/j.engstruct.2017.05.070

Genest C, MacKay J (1986) The joy of copulas: bivariate distributions with uniform marginals. Am Stat 40:280–283. https://doi.org/10.2307/2684602

Genest C, Rivest L (1993) Statistical-Inference procedures for bivariate archimedean copulas. J Am Stat Assoc 88:1034–1043. https://doi.org/10.2307/2290796

Huang S, Li Q, Shu Z, Chan PW (2023) Copula-based joint distribution analysis of wind speed and wind direction: wind energy development for Hong Kong. Wind Energy 26:900–922. https://doi.org/10.1002/we.2847

International Electrotechnical Commission (IEC) (2022) Wind energy generation systems-Part 50–1: Wind measurement-Application of meteorological mast, nacelle and spinner mounted instruments

Jenkinson AF (1955) The frequency distribution of the annual maximum (or minimum) values of meteorological elements. Q J R Meteorol Soc 81:158–171. https://doi.org/10.1002/qj.49708134804

Li L, Kareem A, Xiao Y et al (2015) A comparative study of field measurements of the turbulence characteristics of typhoon and hurricane winds. J Wind Eng Ind Aerodyn 140:49–66. https://doi.org/10.1016/j.jweia.2014.12.008

Li T, Guo S, Liu Z et al (2016) Bivariate design flood quantile selection using copulas. Hydrol Res 48:997–1013. https://doi.org/10.2166/nh.2016.049

Liao H, Jing H, Ma C et al (2020) Field measurement study on turbulence field by wind tower and windcube lidar in mountain Valley. J Wind Eng Ind Aerodyn 197:104090. https://doi.org/10.1016/j.jweia.2019.104090

Ministry of Transport of the People's Republic of China (2015) General Specifications for Design of Highway Bridges and Culverts (JTG D60-2015). Beijing

Nagler T, Czado C (2016) Evading the curse of dimensionality in nonparametric density estimation with simplified vine copulas. J Multivar Anal 151:69–89. https://doi.org/10.1016/j.jmva.2016.07.003

Nelsen RB (2006) An introduction to copulas, 2 edn. Springer, New York Berlin Heidelberg

Nikoloulopoulos AK (2013) Copula-based models for multivariate discrete response data. In: Jaworski P, Durante F, Härdle WK (eds) Copulae in mathematical and quantitative finance. Springer, Berlin, Heidelberg, pp 231–249. https://doi.org/10.1007/978-3-642-35407-6_11

Panamtash H, Zhou Q, Hong T et al (2020) A copula-based bayesian method for probabilistic solar power forecasting. Sol Energy 196:336–345. https://doi.org/10.1016/j.solener.2019.11.079

Ramírez AF, Valencia CF, Cabrales S, Ramírez CG (2021) Simulation of photo-voltaic power generation using copula autoregressive models for solar irradiance and air temperature time series. Renewable Energy 175:44–67. https://doi.org/10.1016/j.renene.2021.04.115

Riera JD, Nanni LF (1989) Pilot study of extreme wind velocities in a mixed climate considering wind orientation. J Wind Eng Ind Aerodyn 32:11–20. https://doi.org/10.1016/0167-6105(89)90012-3

Salvadori G, Tomasicchio GR, D'Alessandro F (2013) Multivariate approach to design coastal and off-shore structures. J Coastal Res 386–391. https://doi.org/10.2112/SI65-066.1

Salvadori G, Durante F, Tomasicchio GR, D'Alessandro F (2015) Practical guidelines for the multivariate assessment of the structural risk in coastal and off-shore engineering. Coast Eng 95:77–83. https://doi.org/10.1016/j.coastaleng.2014.09.007

Sklar M (1959) Fonctions de répartition à N dimensions et leurs Marges. Ann De l'ISUP VIII:229–231

Valipour M (2015) Importance of solar radiation, temperature, relative humidity, and wind speed for calculation of reference evapotranspiration. Arch Agron Soil Sci 61:239–255. https://doi.org/10.1080/03650340.2014.925107

Yet ZR, Masseran N, Ariff NM (2019) Probabilistic distribution of solar irradiation frequency using copulas. AIP Conf Proc 2111:020023. https://doi.org/10.1063/1.5111230

Yin J, Guo S, Liu Z et al (2017) Bivariate seasonal design flood Estimation based on copulas. J Hydrol Eng 22:05017028. https://doi.org/10.1061/(ASCE)HE.1943-5584.0001594

Yu C, Li Y, Zhang M et al (2019) Wind characteristics along a Bridge catwalk in a deep-cutting gorge from field measurements. J Wind Eng Ind Aerodyn 186:94–104. https://doi.org/10.1016/j.jweia.2018.12.022

Zhang H, Liu Y, Deng Y (2021a) Temperature gradient modeling of a steel box-girder suspension Bridge using copulas probabilistic method and field monitoring. Adv Struct Eng 24:947–961. https://doi.org/10.1177/1369433220971779

Zhang J, Zhang M, Li Y et al (2021b) Comparison of wind characteristics in different directions of deep-cut Gorges based on field measurements. J Wind Eng Ind Aerodyn 212:104595. https://doi.org/10.1016/j.jweia.2021.104595

Zhang J, Zhang M, Jiang X et al (2022) Pair-Copula-based trivariate joint probability model of wind speed, wind direction and angle of attack. J Wind Eng Ind Aerodyn 225:105010. https://doi.org/10.1016/j.jweia.2022.105010

Zhang M, Zhang J, Chen H et al (2023a) Probabilistic wind spectrum model based on correlation of wind parameters in mountainous areas: focusing on von Karman spectrum. J Wind Eng Ind Aerodyn 234:105337. https://doi.org/10.1016/j.jweia.2023.105337

Zhang M, Zhang J, Jiang F et al (2023b) Combined wind profile characteristics based on wind parameters joint probability model in a mountainous gorge. Nat Hazards 115:709–733. https://doi.org/10.1007/s11069-022-05571-w